Batteries & Supercaps

Research Article
doi.org/10.1002/batt.202400358

Chemistry Europe
European Chemical Societies Publishing

www.batteries-supercaps.org

Development and Upscaling of a Waterborne Formulation for High-Energy Density NMC811 Cathodes

Susan Sananes-Israel,[a] Idoia Urdampilleta,[a, b] Galyna Kvasha,[a] Imanol Landa-Medrano,[a] and Iratxe de Meatza*[a, c]

The pursuit of high-energy lithium-ion cells has led to an increase in the fraction of nickel in the $LiNi_xMn_yCo_zO_2$ (NMC, with $x+y+z=1$) layered oxide, a state-of-the-art cathode material in electric vehicles. NMC is usually processed using organic solvents that are non-sustainable. Nevertheless, increasing the Ni fraction entails a decrease in the electrode stability and the processability of this material in water. In this work, high-nickel NMC materials have been subjected to water processing. In an initial stage, water sensitivity of the materials has been studied. Then, the formulation has been adapted to enhance the NMC fraction without penalizations in the electrochemical performance and compared to an organic solvent-based formulation. The recipe developed, consisting of 93% of NMC, has been successfully upscaled to a semi-industrial coating line. The pH buffering has been observed as a critical step to mitigate lithium leaching and implement this process in an industrial environment. The obtained electrodes have been tested in single-layer pouch cells using silicon-based negative electrodes, also processable in water-based slurries. The resulting cells provide limited cycling life due to the low cyclability of the negative electrode but evidence that it is industrially viable to manufacture high-energy cells consisting only of water-processed electrodes.

Introduction

Lithium-ion batteries (LIBs) have been the game changer allowing the exploitation of autonomous small-scale electric devices, such as laptops and cell phones.[1,2] Furthermore, the dependence on fossil fuels has decreased in the last years due to the development and commercialization of electric vehicles (EVs).[3] Despite the rapid growth of the electric fleet on our roads,[4] there are still some doubts regarding the long charging time necessary to fully recharge their batteries and their limited driving range. The finding of materials that allow fast charge is one hot topic in the battery research community and, on the other hand, range anxiety has been faced by developing high energy density materials.[5,6] Among these materials, different alternatives have been identified for anodes and cathodes; the state-of-the-art graphite negative electrode has been partially replaced by silicon-based materials,[7] while most electric cars consist of layered metal oxides as active materials in the positive electrode.[8] $LiNi_{0.8}Co_{0.15}Al_{0.05}O_2$ (NCA) and $LiNi_{0.8}Mn_{0.1}Co_{0.1}O_2$ (NMC811, hereafter NMC) are the most popular options for high energy applications due to their high capacity (200 $mAh \cdot g^{-1}$) and working potential (~3.7 V vs Li/Li^+).[9,10] Both have lower cobalt and higher nickel content than the original $LiNi_{0.33}Mn_{0.33}Co_{0.33}O_2$ (NMC111), leading to higher specific capacity.[11,12] However, the price to be paid for this higher capacity is a decrease in thermal and electrochemical stability,[13] ultimately leading to lower safety. In any case, they have been implemented in most of the electric vehicles in the last years.[8]

As already mentioned, graphite is a state-of-the-art anode material. Its low working potential (~0.1 V vs Li/Li^+), relatively high capacity (~360 $mAh \cdot g^{-1}$), limited volume change upon cycling, and well-implemented mining and production industry make it an ideal candidate for this role.[11,14] Nevertheless, silicon-based materials have been studied as an alternative to graphite to further increase the energy density of the cells. Pure silicon has a specific capacity of ~3600 $mAh \cdot g^{-1}$ (based on the lithiation to $Li_{3.75}Si$[15]), but such a high capacity is associated with a volumetric expansion of 300%, which makes it difficult to maintain the structural integrity of electrodes based on pure silicon.[16,17] Moreover, the solid-electrolyte interphase (SEI)[18] is hardly kept unfractured upon these lithiation-delithiation steps, involving the consumption of more lithium in the re-building of this SEI.[19] As an alternative, silicon (sub)oxides[20] and silicon-carbon composites[21] have been studied. These materials have a lower capacity (around 1200–1500 $mAh \cdot g^{-1}$[17,22]) and, there-

[a] Dr. S. Sananes-Israel, I. Urdampilleta, G. Kvasha, I. Landa-Medrano, I. de Meatza
CIDETEC, Basque Research and Technology Alliance (BRTA)
Po. Miramón 196, 20014 Donostia-San Sebastián, Spain
E-mail: imeatza@cidetec.es
idmeatza001@ikasle.ehu.eus
imeatza@gmail.com

[b] I. Urdampilleta
Department of Applied Chemistry
University of Basque Country (UPV/EHU)
20018 Donostia-San Sebastian, Spain

[c] I. de Meatza
Department of Organic and Inorganic Chemistry
University of Basque Country (UPV/EHU)
48080 Bilbao, Spain

Supporting information for this article is available on the WWW under https://doi.org/10.1002/batt.202400358

fore, they undergo a lower volumetric expansion. However, it is still difficult to find electrodes consisting of pure silicon (sub)oxides or silicon/carbon composites, and are usually found in commercially available LIBs as additives (< 10 wt.% Si).[8] The processing of graphite and silicon-based materials is industrially performed using water as a solvent,[23] in which the different components of the electrodes are dispersed. Then, the copper current collectors are coated with this dispersion and the solvent is evaporated using ovens.[24]

The use of water is not industrially implemented for most of the cases when the positive electrode is manufactured.[3,23] In this case, the most popular solvent is N-methyl-pyrrolidone (NMP), which is harmful to humans, needs higher temperatures for evaporation, and is more expensive and must be recycled.[24–26] The concern of public institutions in terms of sustainability related to batteries and EVs is evident considering the last regulations,[27] and the exponential replacement of combustion engine-based vehicles by EVs[28] makes it necessary to make the production processes of these batteries more sustainable. As claimed by Greta Thunberg in a phrase that has become popular, there is no planet B;[29] thus, minimizing the environmental impact of our activity is of major importance. This has been the driving motivation for this work.

In any case, the replacement of NMP by water in the industrial production of NMC cathodes is not trivial. A recent review by Li et al.[25] summarized the main challenges: (1) replacing polyvinylidene fluoride (PVDF) with water-soluble or waterborne binders; (2) removing high residual moisture in electrodes processed in water due to hydrophilic binders; (3) impeding the agglomeration of active material and conductive-additive particles in water; (4) inferior wetting on the aluminum current collector due to the high surface tension of water; (5) avoiding corrosion on the aluminum current collector due to the basicity of the aqueous slurries; and (6) minimizing the leaching of lithium and transition metals from cathode active materials when exposed to water, which may lead to surface reconstruction.

PVDF is the most widely used binder for organic formulation, but its performance is worse when using water as the solvent for the slurry.[30] Furthermore, it can undergo decomposition to form HF, which reacts with the lithium in the cell causing its degradation.[30] On the other hand, waterborne binders are hydrophilic, and the electrodes prepared using them must be carefully dried (100–120 °C) to avoid the presence of water traces before assembling the cells.[23] Nevertheless, the equilibrium vapor pressure is 35 times higher for water than for NMP, which means water evaporates faster, and drying times are, therefore, shorter.[31] This advantage, however, can become a disadvantage as cracking of the electrode upon solvent evaporation represents a new challenge.[32] Furthermore, the surface tension of water is higher than that of the organic solvents and the wetting of the aluminum current collectors is less efficient in aqueous media.[33] These two challenges, which affect more severely high-loading electrodes, can be simultaneously tackled by reducing the surface tension of the aqueous dispersion by adding isopropyl alcohol (IPA).[32] The difficulties associated with the interaction between the aqueous slurry and the current collector are not limited to the proper wetting, as corrosion of aluminum is another factor that must be considered. As studied by Sahore et al.[34] the basicity of the aqueous slurry leads to the formation of hydrogen gas, which causes cracking during the drying step. They evidenced that corrosion was the most significant factor influencing the formation of cracks in the electrode. Reducing the drying stress and improving the binding network resulted in mitigating this issue. Also in their study, the addition of IPA contributed to improving the quality of the coatings. The improvement of the binding properties to mitigate cracking was also pursued by Demiryürek et al.[35] In their work, different ratios of carboxymethyl cellulose (CMC), styrene-butadiene rubber (SBR), and poly(ethylene oxide) (PEO) were compared to optimize a $LiNi_{0.5}Mn_{0.3}Co_{0.2}O_2$ (NMC532) formulation that was later upscaled to a roll-to-roll pilot-scale production line. The electrodes manufactured were tested in pouch cell format with remarkable electrochemical performance.

Another challenge to obtaining high-quality coatings in aqueous media is the formation of agglomerates. Usual cathode formulations consist of active materials, conductive additives, and binding agents,[25] and in many cases, the active materials are covered by conductive or protective layers to improve their performance and stability.[36,37] In addition, the conductive additive is a carbon-based component, such as conductive carbon, nanotubes, or nanofibers.[37–39] Thus, both the surface of the active material and the conductive additive(s) are hydrophobic, which difficult their adequate dispersion in the aqueous slurry and leads to particle agglomeration.[23] The use of surfactants can mitigate this issue.[40]

The last difficulty listed in the review by Li et al.[25] was the leaching of lithium and transition metals from the active materials. This inconvenience is not limited to NMC, as this phenomenon has also been observed when NCA is subjected to aqueous processing.[41,42] Hoffmann et al. published an extensive research work related to the processing of layered transition metal oxides divided into two parts. In the first one,[41] NMC materials with different Ni:Mn:Co ratios (NMC111, NMC622, and NMC811) and NCA were subjected to processing in aqueous slurries under the same conditions to allow the direct comparison between them. An increase in the pH of the slurry was observed with increasing the Ni fraction in the NMC series, in parallel with a decrease in the electrochemical performance in comparison to the NMP-processed electrodes with the same materials. Lithium leaching was attributed to a nickel-driven process, which was time-dependent, i.e., lithium (and transition metal) leaching was aggravated by increasing the processing time. Nevertheless, the difference between water- and NMP-based NMC electrodes decreased during the first galvanostatic cycles, which was ascribed to a reversible Li^+/H^+-exchange mechanism. The influence of water processing on NCA was even more dramatic, as leaching was aggravated in the presence of aluminum: the reversibility observed for NMC-based electrodes was not observed in this case. In the second part of the research work,[42] the focus was put on the processing of NCA. The analysis of NCA in contact with water for different exposure times revealed the appearance of new

surface species on NCA (Li_2CO_3, LiOH, and aluminum compounds) with increasing the exposition time. These compounds were formed due to the presence of chemisorbed CO_2, basic nickel carbonate, and $NiOOH^-$ like species. Lithium was captured (leached) as Li_2CO_3 and LiOH, hindering the electrochemical performance of the NCA by increasing the exposure time to water. These surface degradation components in NMC were characterized by Azhari et al.[43] using X-ray photoelectron spectroscopy (XPS) and transmission electron microscopy (TEM). They evidenced that the mechanical stress caused during the drying step in combination with these surface species increases the susceptibility to intergranular fracture, which ultimately leads to capacity fade and impedance growth when subjected to electrochemical testing. Finally, in a remarkable work, Neidhart et al. evidenced that the use of binder gradients could be the key to enabling high-loading NMC electrodes.[44]

In this work, the optimization and upscaling of a water-based high-Ni NMC electrode formulation have been achieved. Initially, the optimum combination of NMC and additives has been investigated, and the upscaling of the formulation developed has been performed at a pilot scale with a semi-industrial roll-to-roll coating line. The recipe has been adapted as new challenges have arisen during the upscaling step. In all cases, the water-processed electrodes have been compared with organic-processed. The cathodes prepared in the coating line were used to assemble high-energy pouch cells with silicon-based anodes. This work aims to provide guidelines on the water-processing of NMC materials and prove that aqueous-based routes for cathode manufacturing can be upscaled and provide successful electrochemical performance.

Experimental Section

Electrode Preparation

The water-based cathodes in this study consisted of $LiNi_{0.83}Mn_{0.07}Co_{0.1}O_2$ (NMC83, Ni83%, POSCO) as the active material. At a preliminary stage, $LiNi_{0.8}Mn_{0.1}Co_{0.1}O_2$ (NMC811, T81R, Targray) was also evaluated as a candidate for this study. Conductive carbon (C-NERGY Super C45 from IMERYS Carbon & Graphite), carboxymethyl cellulose (CMC, Walocel CRT2000PA, DOW), and acrylic binder (AX-A871 from Zeon, 40 wt.% concentration) were used as conducting, dispersing, and binding additives, respectively. These materials were mixed in water using a mechanical mixer (RW 20 digital, IKA). The slurries consisted of 50 g of solids and the solid-to-liquid ratio was around 1/0.7 (it was slightly changed depending on the sample. See section 3 for further detail), corresponding to 41 wt.% solids. The pH of the slurry was adjusted by H_3PO_4 (PA, 50 wt.% in water, Sharlau) addition. The amount of PA was fixed to NMC:PA weight ratio = 1:0.08. On the other hand, the organic-based electrodes consisted of the same NMC but different additives. Conductive carbon (C-NERGY Super C65 from IMERYS Carbon & Graphite) and polyvinylidene fluoride (PVDF, Solef® 5130, Solvay) were used as the conducting and binding additives, respectively. These components were dispersed in N-methyl pyrrolidone (NMP, Synthesis grade, Scharlab). The solids content of this slurry was also 50 g, and the solid/liquid ratio was 1/0.55. These slurries were coated onto a 15 μm-thick aluminum foil (Hydro) by a doctor blade coater and dried in a convection oven at 60 °C (water-based) or 110 °C (NMP-based). The target loading of these coatings was 4 $mAh \cdot cm^{-2}$, using 200 $mAh \cdot g^{-1}$ as the reference capacity for the loading estimations, close to or even slightly above the optimum value reported in the literature.[32,35] Afterward, NMC coatings were calendered to 3.2 $g \cdot cm^{-3}$ using a table-top calendering machine (DMP solutions). The loading was confirmed by punching and weighting 16.6 mm-diameter disks using an EL-Cut device from EL-Cell, while the density was calculated based on the areal weight and thickness of the electrodes by means of a Mitutoyo 389–271 C micrometer.

Electrode labeling is "NMCXX_org/aq_YY%": XX for NMC811 or NMC83 followed by "org" or "aq" for NMP- or water-processing, respectively, and YY for the active material amount in the electrode (e.g. NMC83_aq_93 for NMC83 water-processed with 93% of active material in the formulation).

The graphite anodes used in this study were also prepared at the laboratory scale, following the same protocol as for the laboratory-scale cathodes. They consisted of 94% graphite (MEG 2C, SGL Carbon), 2% C45, 2% CMC, and 2% styrene-butadiene rubber (SBR, BM-451B, ZEON). These components were dispersed in water and coated onto an 8 μm-thick copper foil (Furukawa). The target loading was 4.4 $mAh \cdot cm^{-2}$ based on a specific capacity of 355 $mAh \cdot g^{-1}$. Graphite anode is labeled "Gr".

The cathode recipe upscaled to a semi-industrial roll-to-roll coating line (Basecoater, Coatema) was the one providing the best performance at the laboratory scale. In parallel, the NMP-based slurry was also upscaled. Both the solid-to-liquid ratios and the target loadings were the same as at the laboratory scale. The loading of the coating was adjusted using a knife system with a variable gap. The solvent was evaporated by going through three consecutive convection ovens (3 meters total). The temperatures of these three zones were 50 °C, 60 °C and 70 °C for the evaporation of water, while to evaporate NMP they were adjusted to 105 °C, 115 °C and 120 °C. The single-side coatings obtained were calendered to 3.2 $g \cdot cm^{-3}$ using a semi-industrial calendaring machine (LDHY 400-N45, Naknor).

The anodes for the single-layer pouch cells were prepared by VARTA Innovation. They consisted of ~9% of Si and ~91% of graphite active material. The developed formulation consisted of 90% (M0366, SGL Carbon), 1% C65, 4% CMC, and 5% styrene-butadiene rubber (SBR, BM-451B, ZEON). The loading of the electrodes was 4.4 $mAh \cdot cm^{-2}$ based on a specific capacity of 676 $mAh \cdot g^{-1}$ for the Si–Gr mix. They were received calendered to a density of 1.5 $g \cdot cm^{-3}$. The Si-based anode is labeled "Si/C".

In this study, we first focused on the water sensitivity towards water processing of the NMC. Then, a screening of different formulations was done and the most promising was scaled-up in a roll-to-roll coating process and validated in pouch cells with Si/C-based anodes for high energy density applications.

Materials Characterization

The rheological behavior of all the slurries was analyzed using a DHR2 rheometer from TA instruments. The adhesion strength of the calendered electrodes to the current collector was measured by a 90° peel test (LS1 model, Lloyd Instruments). The morphology of the active materials and the electrodes was analyzed by means of field emission scanning electron microscopy (FE-SEM, ULTRA plus ZEISS). The samples were prepared in the lab and stuck to the holder using carbon adhesive tape. FE-SEM micrographs at different magnifications (from ×200 to ×10000) were obtained.

Research Article
doi.org/10.1002/batt.202400358
Chemistry Europe
European Chemical Societies Publishing

ICP and pH Measurements

2 g of NMC material were stirred in 20 g of ultra-pure water and the pH was measured at different soaking times. pH measurements were done on solutions exposed to NMC materials using a pH-meter (SensION TM pH 1 from HACH). The pH-electrode used was HACH5212 (WVR) and was calibrated with stock solutions (pH = 4.01, 7, 10) before the measurements. After 24 hours, the material was filtered and dried at 60 °C overnight. The remaining solution was analyzed by ICP-OES (Spectroblue FMX36, METROHM) for the determination of the contents of Li, Co, Mn, and Ni. The operating conditions employed in the ICP-OES analysis were 1300 W RF power, 8 $dm^3 \cdot min^{-1}$ plasma flow, 0.9 $dm^3 \cdot min^{-1}$ auxiliary flow, 0.75 $dm^3 \cdot min^{-1}$ nebulizer flow, 2 $cm^3 \cdot min^{-1}$ sample uptake rate. The measurement was repeated 3 times per sample. Calibration standards were prepared by diluting a stock multi-elemental standard solution (1000 $mg \cdot dm^{-3}$) in 0.2% nitric acid. Samples were diluted to 1:1 for Co, Mn, Ni analysis and to 1:50 for Li analysis. The selected emission lines for the investigated metals were as follows: 670.789 nm for Li, 228.616 nm for Co, 257.611 nm for Mn, and 231.604 nm for Ni. The obtained results were expressed as $mg \cdot L^{-1}$ (for each metal).

Cell Assembly

All the cells in the current study were assembled in a dry room (dew point −40 °C). Before cell assembly, the electrodes were dried at 120 °C under vacuum for 16 hours. The rest of the pouch cell components (separators and aluminum laminated foil (ALF) pouch material (without depth-forming)) were dried at 60 °C under vacuum overnight. Coin cell cases were cleaned with ethanol in an ultrasonic bath for 15 min and dried at 60 °C for 1 h.

The electrochemical performance of the laboratory- and pilot-scale electrodes was characterized in half coin cell (HCC) and full coin cell (FCC) configurations (CR2025, Hohsen). In HCCs, 50 μm-thick lithium discs of 18.2 mm diameter (Albemarle) were used as counter and reference electrodes. The working electrodes were 16.6 mm in diameter. On the other hand, FCCs were assembled using NMC-based positive electrodes (16.6 mm diameter) and graphite-based negative electrodes (17.7 mm diameter). All the cells were assembled using 18.92 mm diameter separators (ceramic coated, Heliumetech HT-180243) soaked with 75 μL of electrolyte. 1 mol·L-1 lithium hexafluorophosphate ($LiPF_6$) in ethylene carbonate (EC)/dimethyl carbonate (DMC) (1:1 in volume) + 10 wt.% fluoroethylene carbonate (FEC), 1.0 wt.% vinylidene carbonate (VC) and 1.0 wt.% lithium bis(trifluoromethanesulfonyl)imide (LiTFSi) electrolyte prepared by UBE Corporation was used in the HCCs, while 1 $mol \cdot L^{-1}$ $LiPF_6$ in EC/DMC/ethyl methyl carbonate (EMC)/FEC (3:3:3:1 in weight) + 2.0 wt.% VC + 0.5 wt.% LiTFSi + 1.0 wt.% trifluoroacetic acid ethyl ester (TFAEt) + 0.5 wt.% difluoroethylene carbonate (F2EC) prepared by Forschungszentrum Jülich was used for the FCCs. This electrolyte formulation was developed in the frame of the project SPIDER. TFAEt is an additive that improve SEI stability and F2EC improves high nickel NMC cathode electrolyte interphase (CEI) stability.[45,46]

The silicon-graphite anode coatings received from VARTA Innovation were validated in HCC. The cell setup was the same as described for the cathode HCCs, including the electrode sizes and the electrolyte. The sole differences for these cells were the separator used (Whatman GF/A) and the amount of electrolyte (100 μL). The selection of Whatman GF/A thick microfiber glass separator is done to avoid possible short circuit generated by the formation of lithium dendrites on the lithium metal anode during HCC testing, which is not the case in FCC testing.

Single-layer pouch cells were assembled with the NMC-based positive electrodes prepared in the coating line and the Si/C-based negative electrodes. The electrodes were cut in a semiautomatic die-cutting machine (MTI Corp). The size of the electrodes was 10×6.1 cm and 9.8×5.9 cm for the anodes and cathodes, respectively. The cathodes were enveloped in separators (ceramic coated, Heliumetech). The enveloped cathode and the anode were aligned using a guiding tool. The electrode flanges were then ultrasonically welded to terminal tabs (100 μm thick, Al (+) and Ni-plated Cu (−)) and then placed between two half-shells of ALF pouch material and heat-sealed on three sides. The cells were filled with 0.65 mL of 1 $mol \cdot L^{-1}$ $LiPF_6$ in EC/DMC/EMC/FEC (3:3:3:1 in weight) + 2.0 wt.% VC + 0.5 wt.% LiTFSi + 1.0 wt.% TFAEt + 0.5 wt.% F2EC. The cells were then vacuum massaged to promote the soaking of the electrodes and the separator with the electrolyte and sealed under vacuum.

The cells were placed between two foams and two stainless steel plates each. 1 N·m of torque pressure was applied to facilitate the contact of the components within the cell.

Electrochemical Testing

The cells were tested in a climatized room (25 ± 1 °C) using a Basytec Test System multichannel potentiostat. The electrochemical experiments with cathode HCCs consisted of galvanostatic cycles between 4.3 V and 2.8 V at different C-rates: one formation cycle at 0.1 C, three cycles at 0.5 C, three cycles at 1 C, three cycles at 2 C, three cycles at 3 C, and continuous 0.33 C cycling until end of life. Symmetric C-rates were used for charge and discharge in the C-rate tests. One cycle at 0.33 C was included as recovery cycle between increasing C-rates. Table S1 details the electrochemical testing protocol used in HCC. The same C-rates were used to test the electrodes prepared at the coating line in FCC configuration, limiting the voltage window to 4.2 and 2.8 V as well as 0.33 C as charge C-rate. On the other hand, verification of the laboratory and pilot-scale electrodes in FCC was performed limiting the rate-capability part of the testing protocol: one cycle at 0.1 C, three at 0.33 C, an aging (resting) step of 24 h, a cycle at 0.33 C to check the capacity fade upon aging, one at 1 C, one at 2 C, one at 3 C, and capacity retention test by subjecting the cells to continuous 0.33 cycling until end of life. For a better understanding, the experiments are summarized in Table 1.

The anodes received from VARTA Innovation were subjected to galvanostatic cycling between 1 V and 0.01 V. The testing protocol consisted of a rate capability test in which the cells were cycled at 0.1 C, 0.33 C, 0.5 C, 1 C, 2 C, and 3 C.

Table 1. Summary of the electrochemical experiments conducted in FCC and pouch cell formats.

Step number	C-rate (Charge/Discharge)	Experiment
1	0.1/0.1 C	Formation
2–4	0.33/0.33 C	Grading
–	–	Aging 24 h
5	0.33/0.33 C	Evaluation of aging
6	0.33/1 C	Rate capability
7	0.33/2 C	Rate capability
8	0.33/3 C	Rate capability
9-end of life	0.33/0.33 C	Cycling – capacity retention

Research Article
doi.org/10.1002/batt.202400358
Chemistry Europe
European Chemical Societies Publishing

Finally, the single-layer pouch cells were cycled between 4.2 and 2.8 V. The cells were initially subjected to a formation cycle at 0.1 C between 4.2 and 2.8 V, followed by 6 h at open circuit voltage at full discharge, and three consecutive cycles at 0.33 C at the same voltage range. After the degassing step, consecutive cycles with charge at 0.33 C and discharge at 0.33 C, 1 C, 2 C, and 3 C rates capability were performed. Afterward, the cells were cycled at 0.33 C until the state of health (SOH) reached 80 %.

Results and Discussion

Effect of the pH on NMC Materials

Two types of commercial NMC materials from different providers were compared (NMC811 and NMC83). Also, the addition of phosphoric acid (PA) with the ratio NMC:PA 1:0.08 (wt.:wt.) was studied. This ratio was selected as it has been shown to maintain the slurry pH below 9 during electrode preparation. PA is a well-studied material that has been proven to enhance the stability of water-processed NMC slurries.[47–49] However, the possible transition metal dissolution or lithium leaching may vary, depending on the active material used. The formation of lithium or transition metal hydroxides can be monitored by measuring the pH of the solution over time. This was done to track and compare the influence of the exposition to water of two commercial NMC materials with or without PA. The results are shown in Figure 1.

It is visible that the NMC811 was more sensitive to water than NMC83, as the initial pH values were higher than 11.5, and a stable pH of 12.3 was reached after only 1 h. The use of PA did not seem to have an influence on this material, except for the first 15 minutes. This showed that the quantity of PA must be adapted depending on the NMC material used. In the case of the NMC83, the pH also raised to more than 12 after 1 h in the absence of PA. This high pH can corrode the aluminum current collector and form H_2 gas,[34] which can be detrimental to the electrode homogeneity and the electrochemical performance. On the contrary, the pH of the solution with NMC83_PA increased gradually with time, evidencing more efficient pH buffering which kept the pH below 10 after 2 h and only increased above 11 after 24 h exposure. NMC83 material might have a protective coating that slows the NMC degradation when exposed to water.

As already discussed, one of the main drawbacks of the water-processed electrodes in comparison to the organic-processed electrodes is the loss of capacity due to lithium leaching and the formation of a passivation layer of Li-based compounds on its surface. Also, transition metals (Co, Mn, and Ni) can be leached from the active material. Therefore, in order to quantify the losses of every element, ICP measurements were conducted on the filtered aqueous solutions exposed to the two NMC materials (NMC83 and NMC811), and the results are displayed in Tables S2 and S3. For both NMC materials, the element with the highest concentration in the solution was Li. Leached transition metals were found only in traces so the focus will be on the lithium concentration. In order to understand the impact of the NMC material on pH evolution, different exposure times were applied, and the soaking solution was analyzed by ICP after 15 min or 24 h exposure. Furthermore, the addition of PA towards leaching was evaluated after 24 h soaking. A summary of the lithium weight fraction leached for the different NMC samples is shown in Table 2. The results are in good agreement with previous pH measurements and show that NMC83 is more suitable for water processing than NMC811, as less lithium was leached when exposed to water (2.4 and 2.8 wt.%, respectively). In addition, the PA allowed for mitigating the amount of lithium leaching, although it was still significant. Kazzazi et al. attributed this to the formation of a protective phosphate layer at the surface of NMC.[47] Besides, a previous work by Wood et al. demonstrated that the higher the nickel content, the higher the lithium leached. Therefore, results with NMC83 are unexpected and it is believed that NMC83 material have a protective coating that slows the NMC degradation when exposed to water.[50] All in all, NMC83 was the NMC material selected for the water-processing study, as it seemed more compatible with water.

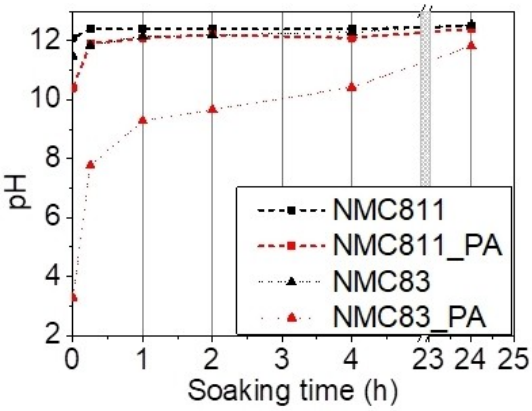

Figure 1. Evolution of the pH after the addition of NMC to water in the presence (red) and absence (black) of phosphoric acid for two NMC materials.

Table 2. Lithium concentration measured by ICP-OES and weight fraction leached from high-Ni NMC for different samples and exposure times.

	NMC83 15 min	NMC83 24 h	NMC83-PA 24 h
Li^+ in solution ($mg \cdot L^{-1}$)	95.52	235.22	135.39
Li leached (wt.%)	1.0	2.4	2.3
	NMC811 15 min	NMC811 24 h	NMC811-PA 24 h
Li^+ in solution ($mg \cdot L^{-1}$)	108	330.23	251.64
Li leached (wt.%)	1.5	2.8	2.6

Research Article
doi.org/10.1002/batt.202400358
Chemistry Europe
European Chemical Societies Publishing

Screening of NMC Water-Based Formulation

The electrode preparation feasibility with the selected NMC83 active material was initially studied with different formulations. This study aimed to maximize the active material content without penalty in terms of electrode manufacturability. The preparation of aqueous-processed NMC electrodes with target loading 4 mAh·cm^{-2} and density 3.2 g·cm^{-3} was pursued with the following NMC/C45/CMC/binder mass fractions: 90/5/2/3 (NMC83_aq_90), 92/3/2/3 (NMC83_aq_92), and 93/2/2/3 (NMC83_aq_93). In parallel, organic-processed NMC electrodes were prepared with 95% NMC, 2% C65, and 3% PVDF as reported in a previous work.[51] Coatings were homogeneous and the adhesion to the current collector was suitable for electrode handling and cell assembly (FE-SEM images and results of the peel test are available in Figure S1).

The rheological behavior of the slurries was analyzed, and the results are shown in Figure 2.

Although the solid-to-liquid (S/L) ratio was adjusted for each of the slurries, it is possible to observe that the higher the C45 fraction, the higher the viscosity of the slurry. This can be concluded by comparing the NMC83_aq_93 and NMC83_aq_90 samples: even if the liquid fraction was higher for the latter (1/0.6 and 1/0.75, respectively), the rheological curves are almost overlapped. Furthermore, the viscosity of NMC83_aq_92 slurry was higher than that of NMC83_aq_90 slurry even though they had similar S/L ratios (1/0.71 and 1/0.75, respectively). This is attributed to the high surface area of the conductive additive, which leads to the adsorption of a higher amount of solvent in its solvation sphere, increasing the viscosity. Finally, even if all the curves show shear thinning behavior, the curves based on organic solvent have a different shape compared with those prepared using water. This will be further discussed later in the "Upscaling to the coating line" subsection.

The electrochemical performance of the three aqueous-processed electrode coatings was initially studied and compared with the organic-processed electrode in half coin cell (HCC) configuration. The cells were subjected to rate capability tests and the results are shown in Figure 3.

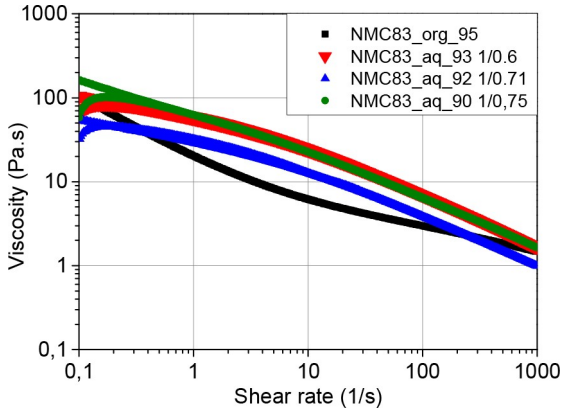

Figure 2. Rheological behavior of the waterborne slurries prepared with different fractions of NMC, C45, CMC, and binder. The curve of the NMP-based formation (unfilled black squares) is included for comparison.

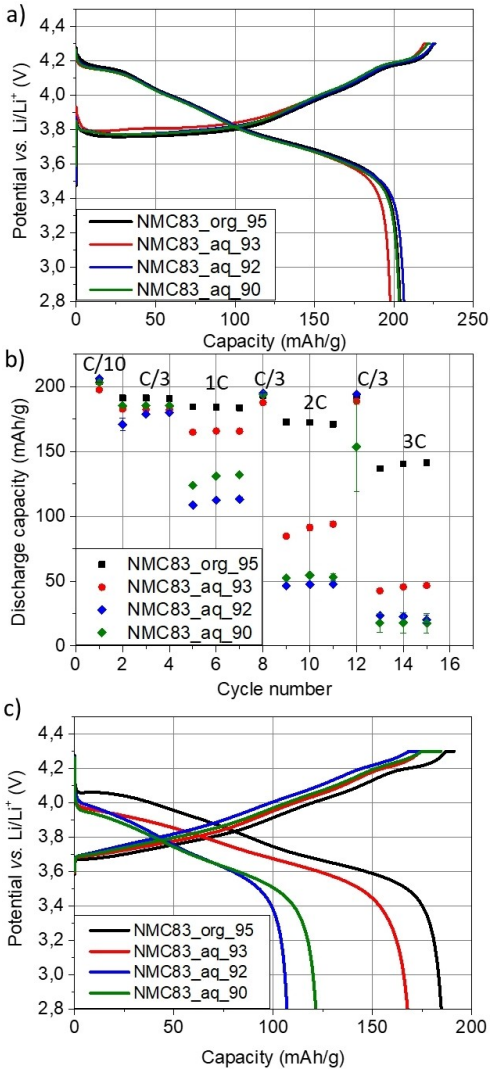

Figure 3. Rate capability experiments with the waterborne NMC cathodes and the NMP-based NMC cathode in HCC. (a) Charge and discharge curves of the formation cycle, (b) specific discharge capacities at different C-rates, and (c) galvanostatic curve at 0.33 C charge and 1 C discharge C-rates.

It can be observed that all the cells presented the same plateaux and, therefore, the water processing did not lead to significant degradation, which could involve the appearance or disappearance of plateaux. These plateaux can be observed by comparing the formation voltage curves of the different cathodes (Figure 3a). The charge reaction was initiated with an extensive plateau at ~3.8 V, followed by two shorter plateaux at 4.0 V and 4.2 V. These plateaux can be attributed to the hexagonal (1) to monoclinic, monoclinic to hexagonal (2), and hexagonal (2) to hexagonal (3) phase transitions.[52] The potential of the plateau at ~3.8 V with the waterborne cathodes was higher for the cathode with the lowest C45 fraction (NMC83_aq_93). The cells with the lowest polarization were those with the organic-processed NMC. The extension of this plateau was similar for all the samples. Nevertheless, there was a difference in the extension of the plateau at ~4.2 V. The cells with the NMC83_org_95 and NMC83_aq_92 had the longest

plateau and, therefore, provided the highest charge capacity. This capacity was lower for the cells with NMC83_aq_90 and NMC83_aq_93. The loss of capacity with two out of three waterborne cathodes suggests that lithium leaching could occur during water processing or that the conductivity of the electrode is lower with water-based formulations. In these two cases, the electrochemical reactions occurred without impediment until all the lithium in the cathode was extracted. At this point, the potential was increased until the cutoff voltage. The curves in the subsequent discharges did not show any polarization but were shorter for the NMC83_aq_93 cells. On the other hand, they were similar to the rest of the samples. The leaching of lithium during processing could be the cause of the lower charge and discharge capacities obtained in the formation step.

The differences in the specific discharge capacities were increased with increasing the current density (Figure 3b). These capacities were approximately 182, 170, and 140 $mAh \cdot g^{-1}$ for the organic-processed electrodes at 1 C, 2 C and 3 C, respectively. Nevertheless, they were decreased to 162, 90, and 45 $mAh \cdot g^{-1}$ respectively for the NMC83_aq_93 sample. The decrease was even more significant for the NMC83_aq_92 and the NMC83_aq_90 samples, despite the higher conductive carbon content. This is in good agreement with an increase in the interfacial resistance of the NMC particles due to water processing, caused by the formation of a passivation layer containing LiOH and Li_2CO_3, as discussed in the Introduction Section. This is evidenced by comparing the galvanostatic curves at 0.33 C charge and 1 C discharge C-rates (Figure 3c). Among the cells with waterborne cathodes, the lowest polarization in the charge at 0.33 C was observed with the NMC83_aq_93 cathodes, followed by NMC83_aq_90 and NMC83_aq_92. This trend was exacerbated in the subsequent discharge to 1 C. Both in the charge and the discharge half-cycles the lowest polarization was observed with the organic-processed NMC electrodes.

The slight differences in the capacity that were observed in the first cycle at 0.1 C between the different samples were attributed to the leaching of lithium. Nevertheless, the significant differences in the performance at higher current densities cannot be ascribed just to this fact. As discussed in the Introduction Section, the lithium leached can be accumulated as lithium carbonate at the surface of the NMC.[42] This degradation route leads to an increase in the interface resistance of the NMC particles, increasing the internal resistance of the cells.

The electrochemical performance of the water-processed electrodes was then studied in full coin cell (FCC) configuration, using graphite as the anode. Contrary to HCCs, there is not an excess of lithium in FCC, and the effects of lithium or transition metal leaching should be more notorious. As the sole source of capacity after cell assembly is the lithium in the NMC, the lithium loss due to leaching during the electrode processing becomes critical. The cells with the different water-based formulations as well as the organic-based standard cathode were subjected to rate capability tests followed by capacity retention tests at 0.33 C. The results are displayed in Figure 4.

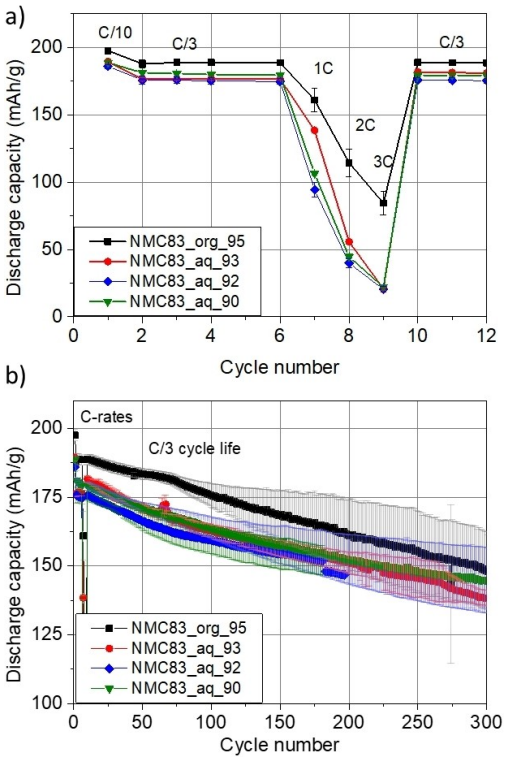

Figure 4. Electrochemical experiments in full coin cells based on graphite anodes and the different water-processed cathodes plus the organic-processed cathode. Specific discharge capacities obtained in the (a) rate capability and (b) cycling tests at 0.33 C. Error bars indicate the standard deviation between the three cells launched per experiment.

Again, the specific capacity was lower for the cells with water-processed electrodes than for those with organic-processed cathodes (Figure 4a). The cells with the organic-processed electrodes provided 197 $mAh \cdot g^{-1}$, while all the cells with the three types of cathodes prepared in aqueous media had a similar capacity: 184 $mAh \cdot g^{-1}$. As expected, lithium leaching during processing affected more significantly the electrochemical performance when using graphite as the negative electrode. Among the cells with aqueous-processed electrodes, those with NMC83_aq_93 provided the best rate capability. The capacity retention was similar for all the cells (Figure 4b), including those consisting of organic-processed electrodes. It can be appreciated that the capacity fade was more pronounced for the cells with NMC83_aq_93 than for those with NMC83_aq_92 and NMC83_aq_90, but it should also be considered that the beginning of life capacity was higher and, at the end-of-life, similar to their counterparts. Thus, to obtain the maximum energy density at the electrode level the formulation selected for the upscaling to the coating line was 93% NMC, 2% C45, 2% CMC, and 3% binder. The electrochemical performances obtained with these materials are in good agreement with previous reports in the literature for NMC83 materials.[53] For example, Radloff et al.[54] obtained capacities of 200 $mAh \cdot g^{-1}$ in the formation cycle for NMC83 electrodes with areal capacity of 3.0 $mAh\,cm^{-2}$. In this work, we demonstrate that, even with electrodes of higher areal capacity

Research Article
doi.org/10.1002/batt.202400358
Chemistry Europe
European Chemical Societies Publishing

(4.0 mAh cm^{-2}), the same initial capacities are obtained. The increase of the electrode loading is critical to obtain high energy density cells. However, the obtained discharge capacities at higher currents are more impacted by the increase on the electrode loading than in previous publications (here 168 mAh·g^{-1} and 180 mAh·g^{-1} obtained by Radloff et al.). In future work, the addition of advanced conducting additive could be a strategy to improve electrode conductivity and C-rate capability. Before the upscaling of water-based formulations, a slurry without PA addition was prepared. The pH before coating was higher than 10 (around 9 for slurries in which PA was added). The resulting electrodes presented "holes" or craters, indicating aluminum corrosion as discussed in the introduction. FE-SEM images revealed a non-homogeneous surface (Figure 5). The use of PA is then critical for the upscaling of aqueous-based NMC slurries.

Upscaling to the Coating Line

The selected recipe including phosphoric acid was upscaled to 1 kg of solids and manufactured at CIDETEC's coating line. Before coating, the rheological behavior of this slurry was analyzed. In parallel, an NMP-based slurry consisting of 1 kg g of solids and another with 50 g of solids were prepared respectively. The rheology curves are shown in Figure 6.

The slurry prepared with organic solvent (50 g solids) in Figure 6a showed the same rheological behavior at low shear rates as the large-size waterborne slurries in Figure 6b. Thus, the susceptibility of the components to disperse in a slurry could be responsible for the differences observed in Figure 6b, and not side reactions during processing such as lithium or transition metals leaching, or the oxidation of the surface of NMC. In organic slurries, there were no differences between large- and small-size slurries, revealing similarities in the mixing processes. On the opposite, the mixing process could be different when working at small- and large-scale with aqueous components, the environment in which carbon and NMC are less susceptible to disperse.[23] The use of PA in the slurry formulation resulted in an increase of the viscosity at low shear rates, indicating a higher stability of aqueous slurries with PA.

The manufactured NMC electrode was evaluated in HCC and FCC formats. In parallel, an NMP-based NMC electrode was prepared at the same coating line and was subjected to the same verification protocols. The electrochemical results are shown in Figure 7. Values of discharge capacity are also available in Table S4 for half and full cells.

Even if the leaching of lithium was mitigated by processing the slurry using phosphoric acid, the capacity of the water-processed electrodes was still below the capacity of the

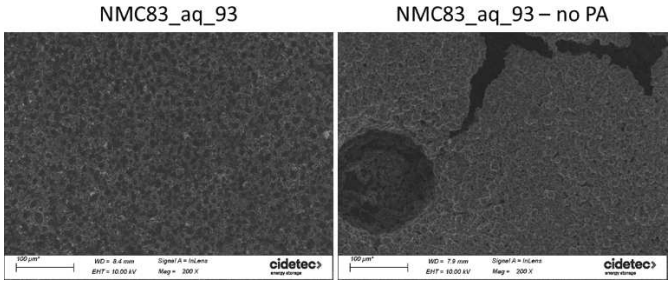

Figure 5. FE-SEM Images of water-based NMC83 slurries with (a) and without (b) H_3PO_4 addition.

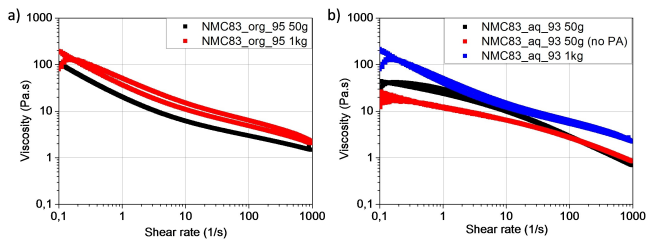

Figure 6. Rheological behavior of the laboratory scale and upscaled slurry with (a) NMP-based formulation with 50 g and 1 kg solids and (b) aqueous-based formulation with and without phosphoric acid at 50 g and 1 kg solids.

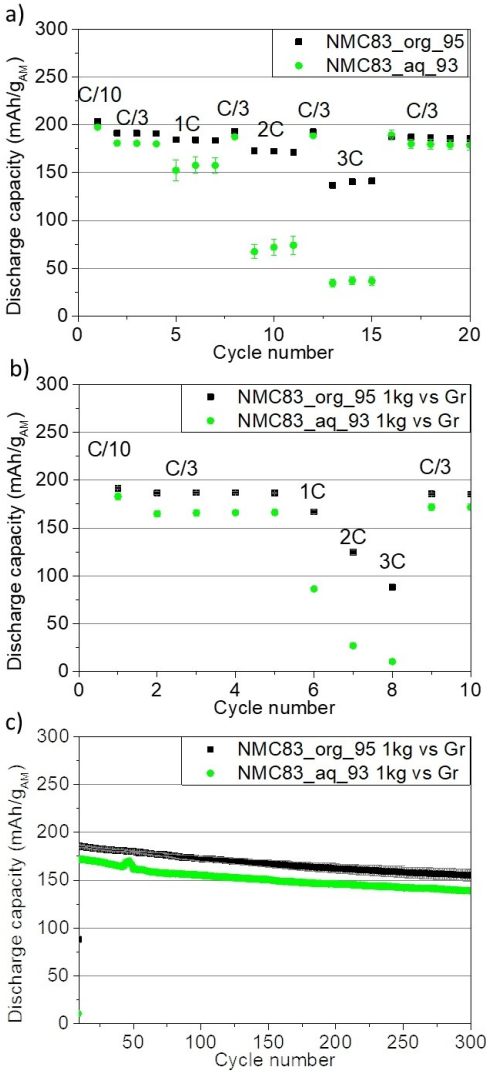

Figure 7. Verification of the NMP- and water-based NMC coatings prepared at the coating line. Rate-capability experiments in (a) HCC and (b) FCC, and (c) discharge capacity evolution upon cycling in FCC.

Research Article
doi.org/10.1002/batt.202400358
Chemistry Europe
European Chemical Societies Publishing

organic-processed electrodes. The differences were much lower at low C-rates: 203 and 197 mAh·g^{-1} (3% difference) for the NMP- and aqueous-based coatings in HCC at 0.1 C, respectively, but they were accentuated at higher C-rates (Figure 7a). The difference in the specific capacity of the electrodes was higher with increasing the C-rate: they grew to 5, 14, 58, and 74% at 0.5 C, 1 C, 2 C, and 3 C, respectively. Cycles at C/3 show a very similar capacity evolution after the C-rate test.

Lithium availability penalized the performance of the water-processed electrodes when tested in FCC (Figure 7b). This time, the capacity was decreased from 198 mAh·g^{-1} (NMP-based) to 183 mAh·g^{-1} (water-based). Also, differences in the C-rate test were observed, as in half cells, with even larger gaps in capacity with the higher C-rate: they grew to 12, 46, 76, and 88% at 0.3 C, 1 C, 2 C, and 3 C, respectively. In addition, absolute discharge capacities obtained were lower in the case of full cells in comparison to half cells for both aqueous and organic formulations. Interestingly, the C/3 discharge capacity of the cells with aqueous NMC83 increased by 10 mAh.g^{-1} after the C-rate test. This increase in capacity can be characteristic of poor lithium diffusion in the first cycles, which can be due to a low electrolyte wettability or the presence of a resistive layer on the surface of the NMC particles. The capacity retention (Figure 7c) was higher for the cell with aqueous-based cathodes and reached 80% of initial capacity after 284 and 300 cycles for NMP- and water-based electrodes, respectively.

When the electrochemical performances of upscaled pilot line electrodes were compared with lab-scale coatings, the results of the formation step were similar for the same formulations (NMP and water-based). The results of the C-rate test (Figure 8a) were very similar for the NMP-based coatings. However, aqueous-based coatings at the laboratory-scale showed higher capacities than upscaled coatings at higher C-rates. The reason for this capacity decrease at high currents can be a higher resistivity of the upscaled electrodes. The loss of lithium was also higher when the coating was upscaled, as lower discharge capacities were obtained in the initial cycles. This is due to longer exposure times of NMC to water when the slurry is upscaled. Also, the coating process is longer in the coating line. These considerations should be taken into account when upscaling water-based formulations.

Despite the decrease in the specific capacity, the performance in the capacity retention test at 0.33 C was successful (Figure 8b), obtaining similar results with water-based and NMP-based electrodes. Upscaled electrodes presented an improvement in the cycle life stability in comparison to the lab-scale ones for both aqueous and organic formulations.

Based on these results, industrial cells based on water-processed NMC83 electrodes would have lower energy density than cells based on NMP-based electrodes. To counteract this penalty, the water-based NMC was tested in full cell configuration using a silicon/graphite composite-based electrode with 650 mAh·g^{-1}. The evaluation of this electrode in HCC is shown in Figure S2.

This time, however, the full cells were not limited to coin cell level: single-layer pouch cells were assembled and tested with the aqueous-processed NMC and the Si/C electrodes.

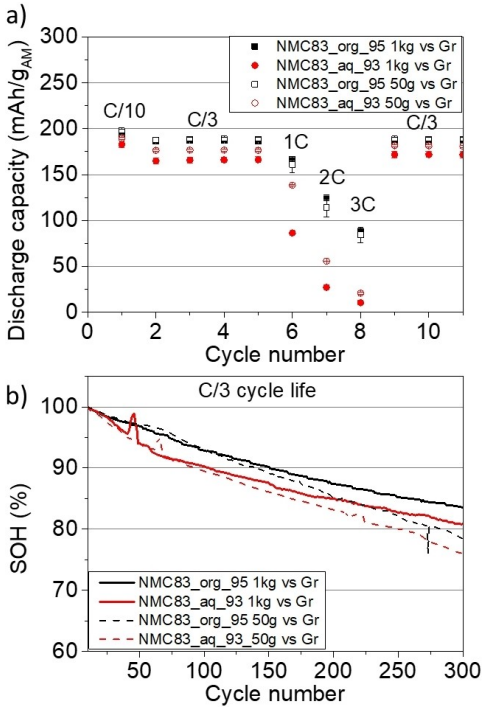

Figure 8. Electrochemical results with the pilot plant and lab-scale cathodes prepared with NMP- and water-based formulations in FCC (a) C-rate capability and (b evolution of relative capacity upon cycle life.

Pouch cells with the same anodes but organic-processed NMC were assembled and tested for comparison. The electrochemical results with these cells are shown in Figure 9.

The formation step consisted of a single cycle at 0.1 C followed by three cycles at 0.33 C. In Figure 9a, the 0.1 C cycle for two cells with each cathode have been represented. Almost no differences were observed between the cells with the organic-based and the aqueous-based cathodes, but there is a slight increase in the voltage polarization difference that suggests that the ion/electronic transport in the aqueous electrodes is affected in comparison with the organic electrodes. The first cycle efficiency was higher for the cells with the NMP-based electrodes than for the aqueous-based electrodes (80.2 vs 79.1%, respectively). The charge and discharge curves did not evidence any defined plateau at first sight.

As could be expected, the rate-capability of the cells with water-based NMC electrodes was still below that of the cells with NMP-based electrodes (Figure 9b). The differences at 0.33, 1 C, 2 C, and 3 C were 2.5, 29, 71, and 80%, respectively. Similarly to the cells in full coin cell format (using graphite anode, in Figure 7b), the rate-capability of the cells with aqueous NMC electrodes was dramatically lower than those with the organic-based NMC. On the other hand, the performance at C/3 (both the initial and the recovered after the C-rate test) with the water-processed cathodes is comparable to the NMP-processed. Also, it is interesting to remark the good reproducibility of the measurement, as the two cells tested per configuration are overlapped. The capacity retention (Figure 9c) was also very similar for the two cells with organic-processed

Research Article
doi.org/10.1002/batt.202400358
Chemistry Europe
European Chemical Societies Publishing

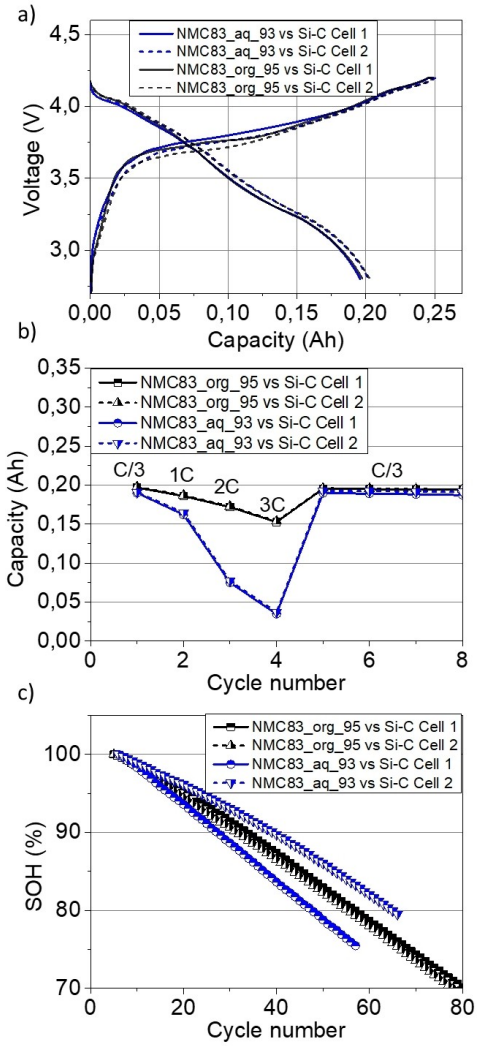

Figure 9. Electrochemical tests with single-layer pouch cells consisting of Si/C anodes and aqueous-processed and organic-processed NMC83 electrodes. (a) Formation curves, (b) rate-capability experiments, and (c) capacity retention during galvanostatic cycling at 0.33 C.

NMC and one cell with aqueous-processed NMC. The performance with the other cell based on aqueous-processed NMC, however, was worse than the rest. The capacity retention of the Si/C anode cells was much lower than in the experiments in FCC using graphite-based anodes. Thus, it is likely that the cycling performance of the single-layer pouch cells was limited by the Si/C in the negative electrode, which is known to have lower cycling stability than pure graphite. Therefore, the lower cycling performance of one of the cells with aqueous-processed NMC could also be attributed to heterogeneities in the negative electrode (loading, porosity, wetting of pores with the electrolyte), as all the results in the study have shown small deviation between the different cells.

Thus, to analyze the electrode reactions, the discharge and charge curves of the formation cycle of full cells with Si/C and graphite anodes have been plotted in dQ/dV vs voltage representation in Figure 8. The capacity has been normalized by the maximum discharge capacity to directly compare the results.

When the formation curves of the graphite and Si/C anode-based cells are normalized (Figure 10a) it is visible that the latter are more polarized. Moreover, as the charge capacity is normalized to the discharge capacity, the normalized charge capacity is higher with the Si/C anodes, which means that the first cycle efficiency is lower with this anode. A more detailed analysis can be performed by analyzing the dQ/dV vs. voltage representation of these curves (Figure 10b). The first feature in the charge curve of the cells with graphite anode has been previously related to the formation of the SEI.[52] This was not observed for the cells with Si/C anode. Thus, the SEI formation dynamics could be different for this composite material. The cells with graphite anode show four defined peaks at 3.60, 3.75, 3.95, and 4.12 V. These reactions were ascribed to the lithiation of graphite and the hexagonal(1)-to-monoclinic, monoclinic-to-hexagonal(2) and hexagonal(2)-to-hexagonal(3) transitions of the NMC, respectively.[52] These reactions appeared at the same voltage in the case of the cells with Si/C anode, but the relative intensity of the lithiation of the peak at 3.60 V was lower. This peak was ascribed to the lithiation of graphite, and in the case of the Si/C anode, the fraction of graphite is lower. Thus, the peak related to its lithiation should also be less intense. In the subsequent discharge, the cells with graphite have signals at 4.0, 3.84, 3.55, and 3.35 V, while the peaks for the Si/C cells are less defined. Furthermore, the peaks are shifted to lower voltages for the cells with Si/C, in good agreement with the higher theoretical redox voltage of silicon (~0.4 V vs. Li/Li^+). A decrease in the current density to better identify the plateaux

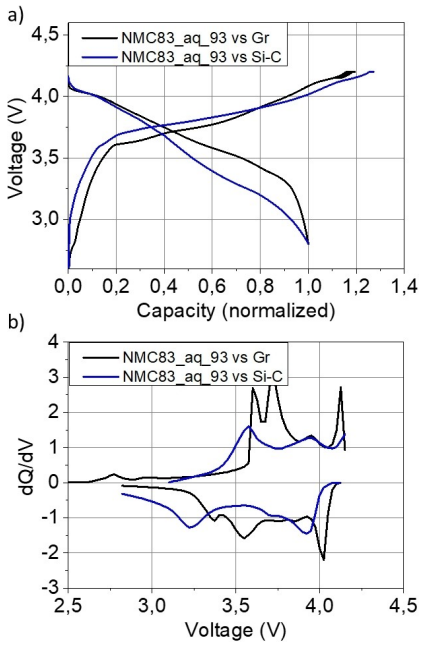

Figure 10. Galvanostatic profile (a) and dQ/dV representation (b) of the formation cycle at 0.1 C of cells consisting of aqueous-based NMC811 and graphite (full coin cell) and Si/C (single-layer pouch cell). The discharge capacity has been normalized to facilitate the analysis.

and gain a deeper understanding of the processes in the cells with Si/C anodes may be advised.

In any case, there is a trade-off between energy density and cycling performance. The ability to assemble high-energy cells using aqueous-processed electrodes has been demonstrated by these cells. Nevertheless, the capacity retention must be improved. A popular strategy, which will be investigated in future work, consists of prelithiating the negative electrodes.[19,55,56]

Conclusions

In this work, the aqueous processing of $LiNi_{0.83}Mn_{0.07}Co_{0.1}O_2$ cathode electrodes has been explored. This material has been evidenced more adequate for water-based processing than another $LiNi_{0.8}Mn_{0.1}Co_{0.1}O_2$ material commercially available, based on ICP and pH analyses. Furthermore, the buffering of the pH using phosphoric acid has been demonstrated as a good strategy to mitigate the leaching of lithium. Once the material was selected, the formulation was analyzed by comparing different active material, conductive additive, and binder fractions, showing that the active material percentage could be increased up to 93 wt.%. The comparison with an organic-processed NMC electrode evidenced that the aqueous-processed electrodes underwent lithium leaching, hindering the electrochemical performance from the first cycle. The rate capability of the aqueous-processed NMC samples was lower than that of the organic-processed NMC samples, which was attributed to a passivation layer on the surface of the NMC particles or a higher resistivity of the coating. Nevertheless, the capacity retention at intermediate current densities was similar with both types of electrodes. The formulation developed at the laboratory was upscaled to an electrode manufacturing line to evidence its viability on an industrially relevant scale. The electrodes obtained with aqueous formulation were used to assemble single-layer pouch cells with Si/C electrodes as anodes. These cells were compared with others consisting of organic-based NMC cathodes. Again, there was a significant penalization on the rate capability at higher C-rates for the cells with aqueous-based NMC cathodes: 2.5, 29, 71, and 80% difference at 0.33, 1 C, 2 C, and 3 C, respectively. Remarkably, the capacity retention was similar with the cells consisting of NMP- and water-based cathodes. The use of high-capacity silicon-based anodes resulted in a decrease in the cycling performance of the cells, but the increase in the energy density achievable with these anodes can be interesting for certain applications. Improvements on the cycle life performance of silicon anodes can be achieved by including carbon additives such as SWCNTs or new electrolyte compositions.[57] Moreover, to go more in depth on the scalability and long-term performance of aqueous-based electrodes, further electrochemical characterization at different temperatures and voltage windows can be carried out. All in all, it has been evidenced that high-Ni NMC high-energy cells can be developed on an industrial scale using both aqueous anodes and cathodes.

Acknowledgements

The authors gratefully acknowledge Judith Pérez, Yahira Ramírez, Andrea Pérez, and Carmen Palacios from CIDETEC for the laboratory-scale electrode preparation, coin cell assembly, ICP analyses, and SEM measurements. In addition, the authors thank the Electrode Manufacturing group at CIDETEC for the pouch cell electrode manufacturing. Furthermore, the authors want to acknowledge the support of SGL Carbon, VARTA Innovation (Dr. Martin Schmuck), and Forschungszentrum Jülich for the Si/C composite, the Si/C anode, and the electrolyte fabrication (Prof. Elie Paillard), respectively, within the project SPIDER (Horizon 2020, grant agreement no. 814389).

Conflict of Interests

The authors declare no conflict of interest.

Data Availability Statement

The data that support the findings of this study are available from the corresponding author upon reasonable request.

Keywords: aqueous processing · high-Ni NMC · Li-ion cells · pouch cells · electrode manufacturing

[1] M. Li, J. Lu, Z. Chen, K. Amine, *Adv. Mater.* **2018**, *30*, 1800561.
[2] L. A. Román-Ramírez, J. Marco, *Appl. Energy* **2022**, *320*, 119305.
[3] S. N. Bryntesen, A. H. Strømman, I. Tolstorebrov, P. R. Shearing, J. J. Lamb, O. Stokke Burheim, *Energies (Basel)* **2021**, *14*, 1406.
[4] M. Fichtner, K. Edström, E. Ayerbe, M. Berecibar, A. Bhowmik, I. E. Castelli, S. Clark, R. Dominko, M. Erakca, A. A. Franco, A. Grimaud, B. Horstmann, A. Latz, H. Lorrmann, M. Meeus, R. Narayan, F. Pammer, J. Ruhland, H. Stein, T. Vegge, M. Weil, *Adv. Energy Mater.* **2022**, *12*, 12102904.
[5] X. G. Yang, C. Y. Wang, *J. Power Sources* **2018**, *402*, 489–498.
[6] M. Dotoli, E. Milo, M. Giuliano, R. Rocca, C. Nervi, M. Baricco, M. Ercole, M. F. Sgroi, *Batteries* **2021**, *7*, 46.
[7] A. A. Tidblad, K. Edström, G. Hernández, I. de Meatza, I. Landa-Medrano, J. Jacas Biendicho, L. Trilla, M. Buysse, M. Ierides, B. P. Horno, Y. Kotak, H. G. Schweiger, D. Koch, B. S. Kotak, *Energies (Basel)* **2021**, *14*, 4223.
[8] M. S. E. Houache, C. H. Yim, Z. Karkar, Y. Abu-Lebdeh, *Batteries* **2022**, *8*, 70.
[9] A. Butt, G. Ali, K. Tul Kubra, R. Sharif, A. Salman, M. Bashir, S. Jamil, *Energy Technol.* **2022**, *10*, 2100775.
[10] Y. Bi, Q. Li, R. Yi, J. Xiao, *J. Electrochem. Soc.* **2022**, *169*, 020521.
[11] J. T. Frith, M. J. Lacey, U. Ulissi, *Nat. Commun.* **2023**, *14*, 420.
[12] M. Fichtner, *Batter Supercaps* **2022**, *5*, e202100224.
[13] R. Lin, S. M. Bak, Y. Shin, R. Zhang, C. Wang, K. Kisslinger, M. Ge, X. Huang, Z. Shadike, A. Pattammattel, H. Yan, Y. Chu, J. Wu, W. Yang, M. S. Whittingham, H. L. Xin, X. Q. Yang, *Nat. Commun.* **2021**, *12*, 2350.
[14] J. Asenbauer, T. Eisenmann, M. Kuenzel, A. Kazzazi, Z. Chen, D. Bresser, *Sustain. Energy Fuels* **2020**, *4*, 5387–5416.
[15] A. Thapa, H. Gao, *J. Electrochem. Soc.* **2024**, *171*, 010504.
[16] Z. Y. Feng, W. J. Peng, Z. X. Wang, H. J. Guo, X. H. Li, G. C. Yan, J. X. Wang, *International Journal of Minerals, Metallurgy and Materials* **2021**, *28*, 1549–1564.
[17] Q. Liu, Y. Hu, X. Yu, Y. Qin, T. Meng, X. Hu, *Nano Research Energy* **2022**, *1*, e9120037.
[18] E. Peled, S. Menkin, *J. Electrochem. Soc.* **2017**, *164*, A1703–A1719.
[19] T. Eguchi, R. Sugawara, Y. Abe, M. Tomioka, S. Kumagai, *Batteries* **2022**, *8*, 49.

[20] Z. Liu, Q. Yu, Y. Zhao, R. He, M. Xu, S. Feng, S. Li, L. Zhou, L. Mai, *Chem. Soc. Rev.* **2019**, *48*, 285–309.
[21] P. Li, H. Kim, S. T. Myung, Y. K. Sun, *Energy Storage Mater.* **2021**, *35*, 550–576.
[22] H. Pegel, O. von Kessel, P. Heugel, T. Deich, J. Tübke, K. P. Birke, D. U. Sauer, *J. Power Sources* **2022**, *537*, 231443.
[23] D. Bresser, D. Buchholz, A. Moretti, A. Varzi, S. Passerini, *Energy Environ. Sci.* **2018**, *11*, 3096–3127.
[24] Y. Liu, R. Zhang, J. Wang, Y. Wang, *iScience* **2021**, *24*, 102332.
[25] J. Li, J. Fleetwood, W. B. Hawley, W. Kays, *Chem. Rev.* **2022**, *122*, 903–956.
[26] I. de Meatza, I. Urdampilleta, I. Boyano, I. Castrillo, I. Landa-Medrano, S. Sananes-Israel, A. Eguia-Barrio, V. Palomares, *J. Electrochem. Soc.* **2023**, *170*, 010527.
[27] European Commission, *Official Journal of the European Union* **n.d.**
[28] Y. Kotak, C. M. Fernández, L. C. Casals, B. S. Kotak, D. Koch, C. Geisbauer, L. Trilla, A. Gómez-Núñez, H. G. Schweiger, *Energies (Basel)* **2021**, *14*, 2217.
[29] NBC News, "'Blah Blah Blah': Greta Thunberg Dismisses World Leaders' Climate Rhetoric," can be found under https://www.youtube.com/watch?v=UryIL4kUcx8, **2023**.
[30] N. Lingappan, L. Kong, M. Pecht, *Renewable Sustainable Energy Rev.* **2021**, *147*, 111227.
[31] N. Susarla, S. Ahmed, D. W. Dees, *J. Power Sources* **2018**, *378*, 660–670.
[32] Z. Du, K. M. Rollag, J. Li, S. J. An, M. Wood, Y. Sheng, P. P. Mukherjee, C. Daniel, D. L. Wood, *J. Power Sources* **2017**, *354*, 200–206.
[33] D. L. Wood, J. Li, C. Daniel, *J. Power Sources* **2015**, *275*, 234–242.
[34] R. Sahore, D. L. Wood, A. Kukay, K. M. Grady, J. Li, I. Belharouak, *ACS Sustain Chem Eng* **2020**, *8*, 3162–3169.
[35] R. Demiryürek, N. Gürbüz, G. Hatipoglu, M. Er, H. Malkoc, O. Guleryuz, G. Uyar, D. Uzun, M. N. Ateş, *Int. J. Energy Res.* **2021**, *45*, 21182–21194.
[36] P. Karayaylali, R. Tatara, Y. Zhang, K. L. Chan, Y. Yu, L. Giordano, F. Maglia, R. Jung, I. Lund, Y. Shao-Horn, *J. Electrochem. Soc.* **2019**, *166*, A1022–A1030.
[37] T. Li, X. Z. Yuan, L. Zhang, D. Song, K. Shi, C. Bock, *Electrochemical Energy Reviews* **2020**, *3*, 43–80.
[38] D. Conor, O.'Brien, R. Collins, A. Holland, *Carbon Nanotubes (CNTs) 2023–2033: Market, Technology, Players*, **2023**.
[39] A. A. Adepoju, Q. L. Williams, *Curr. Appl. Phys.* **2020**, *20*, 1–4.
[40] W. Porcher, B. Lestriez, S. Jouanneau, D. Guyomard, *J. Power Sources* **2010**, *195*, 2835–2843.
[41] M. Hofmann, M. Kapuschinski, U. Guntow, G. A. Giffin, *J. Electrochem. Soc.* **2020**, *167*, 140512.
[42] M. Hofmann, M. Kapuschinski, U. Guntow, G. A. Giffin, *J. Electrochem. Soc.* **2020**, *167*, 140535.
[43] L. Azhari, X. Zhou, B. Sousa, Z. Yang, G. Gao, Y. Wang, *ACS Appl. Mater. Interfaces* **2020**, *12*, 57963–57974.
[44] L. Neidhart, K. Fröhlich, F. Winter, M. Jahn, *Batteries* **2023**, *9*, 171.
[45] H. Tu, S. Li, C. Liu, Z. Luo, L. Ni, Y. Zhang, W. Deng, G. Zou, L. Zhou, H. Hou, X. Ji, *ACS Appl. Mater. Interfaces* **2023**, *15*, 53533–53539.
[46] S. Yang, M. Hao, Z. Wang, Z. Xie, Z. Cai, M. Hu, B. Chen, L. Wang, K. Zhou, *Chem. Eng. J.* **2022**, *435*, DOI 10.1016/j.cej.2022.134897.
[47] A. Kazzazi, D. Bresser, A. Birrozzi, J. Von Zamory, M. Hekmatfar, S. Passerini, *ACS Appl. Mater. Interfaces* **2018**, *10*, 17214–17222.
[48] J. R. Tolchard, P. E. Vullum, B. Arstad, N. P. Wagner, *RSC Sustainability* **2023**, *1*, 378–387.
[49] A. Kukay, R. Sahore, A. Parejiya, W. Blake Hawley, J. Li, D. L. Wood, *J. Colloid Interface Sci.* **2021**, *581*, 635–643.
[50] D. L. Wood, M. Wood, J. Li, Z. Du, R. E. Ruther, K. A. Hays, N. Muralidharan, L. Geng, C. Mao, I. Belharouak, *Energy Storage Mater.* **2020**, *29*, 254–265.
[51] I. de Meatza, I. Landa-Medrano, S. Sananes-Israel, A. Eguia-Barrio, O. Bondarchuk, S. Lijó-Pando, I. Boyano, V. Palomares, T. Rojo, H. J. Grande, I. Urdampilleta, *Batteries* **2022**, *8*, 79.
[52] I. Landa-Medrano, A. Eguia-Barrio, S. Sananes-Israel, S. Lijó-Pando, I. Boyano, F. Alcaide, I. Urdampilleta, I. De Meatza, *J. Electrochem. Soc.* **2020**, *167*, 090528.
[53] A. C. Rolandi, I. De Meatza, N. Casado, M. Forsyth, D. Mecerreyes, C. Pozo-Gonzalo **2024**, DOI 10.1039/d4su00098f.
[54] S. Radloff, G. Carbonari, R. G. Scurtu, M. Hölzle, M. Wohlfahrt-Mehrens, *J. Power Sources* **2023**, *553*, DOI 10.1016/j.jpowsour.2022.232253.
[55] C. Yang, H. Ma, R. Yuan, K. Wang, K. Liu, Y. Long, F. Xu, L. Li, H. Zhang, Y. Zhang, X. Li, H. Wu, *Nat. Energy* **2023**, *8*, 703–713.
[56] L. Jin, C. Shen, Q. Wu, A. Shellikeri, J. Zheng, C. Zhang, J. P. Zheng, *Adv. Sci.* **2021**, *8*, 2005031.
[57] I. Landa-Medrano, I. Urdampilleta, I. Castrillo, H. J. Grande, I. de Meatza, A. Eguia-Barrio, *Energies (Basel)* **2024**, *17*, DOI 10.3390/en17071616.

Manuscript received: May 31, 2024
Revised manuscript received: July 18, 2024
Accepted manuscript online: August 13, 2024
Version of record online: October 16, 2024